This is the accepted manuscript version of:
Tian, H., Huang, F., Zhu, Y., Liu, S., Han, Y., Jaroniec, M., … Liu, J. (2018). The Development of Yolk-Shell-Structured Pd&ZnO@Carbon Submicroreactors with High Selectivity and Stability. Advanced Functional Materials, 28(32), 1801737. doi:10.1002/adfm.201801737

DOI: 10.1002/ ((please add manuscript number))

Article type: Full Paper

The development of yolk-shell structured Pd&ZnO@carbon submicroreactors with high selectivity and stability

Hao Tian, Fei Huang, Yihan Zhu, Shaomin Liu, Yu Han, Mietek Jaroniec, Qihua Yang, Hongyang Liu, G. Q. Max Lu and Jian Liu**

[a] Dr H. Tian, Prof. Q. H. Yang, Prof. J. Liu
State Key Laboratory of Catalysis, iChEM, Dalian Institute of Chemical Physics
Chinese Academy of Sciences
457 Zhongshan Road, Dalian 116023, China
E-mail: jianliu@dicp.ac.cn

[b] Dr H. Tian, Prof. S. M. Liu, Prof. J. Liu
Department of Chemical Engineering, Curtin University
Perth, WA 6845, Australia

[c] F. Huang, Prof. H. Y. Liu
Shenyang National Laboratory for Materials Science, Institute of Metal Research
Chinese Academy of Sciences
72 Wenhua Road, Shenyang 110016, China

Email: liuhy@imr.ac.cn

[d] Dr Y. H. Zhu, Prof. Y. Han
Advanced Membranes and Porous Materials Center, Chemical and Life Science and Engineering Division, King Abdullah University of Science and Technology

Thuwal 23955-6900, Saudi Arabia

[e] Prof. Y. H. Zhu
Department of Chemical Engineering, Zhejiang University of Technology

Hangzhou 310014, China

[f] Prof. M. Jaroniec
Department of Chemistry and Biochemistry, Kent State University, Kent, Ohio 44242, USA

[g] Prof. G. Q. Max Lu

Vice-Chancellor's Office, University of Surrey

Guildford, Surrey, GU2 7XH, United Kingdom

[h] Prof. J. Liu
Department of Chemical and Process Engineering, University of Surrey

Guildford, Surrey, GU2 7XH, UK

E-mail: jian.liu@surrey.ac.uk

Keywords: submicroreactor, yolk-shell, metal–organic frameworks, phenylacetylene hydrogenation, zeolite imidazolate frameworks.

Abstract: Design of multicomponent yolk-shell structures is crucial for the fabrication of micro/nanoreactors for a variety of applications. In this work, we report the rational design and synthesis of yolk-shell structured submicroreactors with loaded metal nanoparticles into ZnO-microporous carbon core-shell structures. The solvothermal treatment and carbonization process of uniform zeolitic imidazolate framework-8 (ZIF-8)@resin polymer core-shell structures led to the generation of yolk-shell structured ZnO@carbon. The synthesis conditions were optimized to track the evolution of ZIF-8 in a confined space of resin polymer as a submicroreactor itself. It has been found that nanoribbon evolution occurs via the formation of the intermediate needle-like particles. The Pd&ZnO@carbon submicroreactor is shown to be a highly selective catalyst (selectivity >99%) for hydrogenation of phenylacetylene to phenylethylene. The excellent performance of Pd&ZnO@carbon particles is evidenced by higher conversion and selectivity than that of Pd/ZnO and Pd/C with similar Pd loading. Furthermore, Pd&ZnO@carbon submicroreactors showed superior catalytic stability, and no deactivation after 25 hours of reaction. The proposed strategy is promising for the design of multifunctional micro/nanoreactors or nanocontainers for construction of artificial cells.

1. Introduction

The design of appropriate reactors is one of very important steps in chemical reaction engineering. The flow dynamics, mass transfer, heat transfer, and reaction kinetics are of great significance for performance of reactors with optimal operating conditions. With the development of nanotechnology, the design and fabrication of reactors from meter scale to micro and nano scale becomes possible.

In the area of materials sciences, the yolk-shell structures with tailored physical and chemical properties have showed great potential in a variety of applications including catalysis, drug release and delivery, energy storage and conversion. [1-6] In particular, the yolk-shell structured nanoparticles are ideal for micro/nanoreactors because they can mimic the structure of living cells able to achieve high efficiency and superior selectivity. However, these artificial cells in addition to high efficiency and super selectivity show excellent stability against sintering at high temperatures. The yolk-shell nanoparticles with distinctive structures and tunable functionalities in both core and shell have been fabricated by selective-etching, soft-templating, Ostwald ripening, ship-in-bottle methods, galvanic replacement method and Kirkendall effect based methods. [7-12] However, there is still a great challenge in designing micro/nanoreactors with precisely controlled composition and selective active sites suitable for cooperative catalysis, coupling and Cascade reactions. As compared to the chemical processes in the meter-scale reactors, there is still a great challenge to study chemical reactions at the nanoscale by monitoring the transfer of reactants and products, heat transfer, and reaction kinetics.

As one of the representative class of metal organic frameworks (MOFs), zeolite imidazolate frameworks (ZIFs) have been commonly used as heterogeneous catalysts because of uniform pore size, well-controlled morphology and good chemical stability.[13-17] Recent efforts have been focused on the design of nanocatalysts at the atomic level on the basis of MOFs.[18-36] For example, Tang and co-workers reported a stable sandwich structure of MOF@Pt@MOF with superior efficiency and selectivity for hydrogenation of α,β-unsaturated aldehydes.[25] Telfer et al. reported the ZIF-derived hollow carbon capsules with confined monometallic or bimetallic nanoparticles and showed that the formation of hollow structures can prevent sintering and detachment of nanoparticles, and simultaneously assure the efficient mass transport and excellent catalytic activity for hydrogenation of nitroarenes.[28] Followed up this work, the same group also developed a general synthetic strategy to encapsulate multi-metallic particles in the porous carbon framework, which exhibited superior electrocatalytic properties.[29]

In our previous work, we reported the fabrication of monodisperse resorcinol-formaldehyde resin and carbon spheres via the extended Stöber method.[37] Based on the recent developments in the area of carbon spheres,[38-49] the versatile technique was used for the fabrication of core–shell and yolk–shell metal oxide-carbon composites with unique core@void@shell structures and various morphologies such as polymer@polymer,[40] Ag@polymer,[41] α-Fe_2O_3 nanospindle@polymer[42] and Fe_2O_3box@polymer[43]. In addition, when metal nanoparticles such as Ag, Pt[41, 44] are introduced into carbon spheres, it is interesting to find that hollow carbon frameworks are generated because these metal nanoparticles could probably catalyze the conversion of carbon spheres to hollow structures during pyrolysis. However, the detailed mechanism of the structure evolution of carbon spheres is still unclear, the structure of these materials is limited to yolk-shell nanoparticles with similar

compositional and morphological cores and shells, and the control of the shell structure and its thickness is difficult. The main reason is that different materials with distinct physical and chemical properties are difficult to manipulate simultaneously during material synthesis. Besides, it is very important to have separate active nanoparticles to preserve their chemical properties.

Herein, inspired by the Stöber-type synthesis of colloidal polymer spheres, we report a spontaneous phase transformation of the ZIF-8@resin polymer core-shell structures to ZnO@polymer yolk-shell structures under mild solvothermal conditions. Coating resin polymer on the surface of ZIF-8 creates a "nanoreactor", in which the aforementioned phase transformation takes place. Besides, this method could also be extended to control the morphology of the internal core, ZnO, and the thickness of the surrounding shell. In addition, Pd metal nanoparticles can be encapsulated within the carbon framework. The catalytic activity of the resulting Pd&ZnO@carbon particles was evaluated in a selective hydrogenation of phenylacetylene to phenylethylene. These distinctive features of the Pd&ZnO@carbon particles are concluded as follows: i) a unique reaction environment is provided for reactant accumulation in heterogeneous catalysis due to the void between ZnO core and carbon shell, ii) a basic atmosphere is fabricated through the in-situ growth of ZnO core for easy desorption of phenylethylene and avoiding over hydrogenation; iii) the catalytic core nanoparticles can be protected via the outer carbon shell by suppressing their agglomeration. Our synthetic strategy empowers the rational design of multifunctional catalysts with enhanced chemical properties and the void space between the core and shell providing sufficient space to host many cargos as micro/nanoreactor or nanocontainer for various applications.

2. Results and Discussions

2.1. Structural analysis

The synthesis strategy of yolk-shell structured ZnO/carbon (ZC) is schematically depicted in Scheme 1a. Two methanol solutions of zinc nitrate hexahydrate ($Zn(NO_3)_2 \cdot 6H_2O$) and 2-methylimidazole (HMI) were mixed for 24 h at room temperature to generate uniform ZIF-8 particles as templates. In the first step, the extended Stöber coating method was used to deposit polymer layer on the surface of ZIF-8. After generating highly uniform ZIF-8@polymer core-shell structures, hydrothermal treatment was used to prepare the yolk-shell structured ZnO@polymer (ZP). Carbonization of these yolk-shell ZP structures under nitrogen atmosphere generated the yolk-shell structured ZnO@carbon (ZC). In order to investigate the effect of Pd metal catalysts in these submicroreactors, Scheme 1b presents the introduction of Pd metal nanoparticles into the yolk-shell structured ZnO@carbon. A wet chemical reduction method was used to form Pd nanoparticles on the ZIF-8 particles by reduction of Pd salts. Aminophenol polymer layer was then coated on the surface of Pd/ZIF-8 particles through the same extended Stöber coating method. Pd&ZnO@carbon particles were then prepared via hydrothermal treatment of Pd&ZIF-8@polymer followed by carbonization.

The structures formed at different experimental conditions were characterized by powder X-ray diffraction (XRD), transmission electron microscopy (TEM) and dark field scanning transmission electron microscopy (HAADF-STEM) imaging and elemental mapping. The XRD pattern of ZIF-8 crystals (Figure S1) agrees well with the previous reports [24,45] and the TEM image of ZIF-8 particles (Figure 1a) show a polyhedral structure with a smooth surface and average particle size of about 300 nm. After coating polymer layer to form ZIF-8@polymer core-shell structure, the particles still remain polyhedral shape but exhibit a rougher surface, as shown in Figure 1b. Figure 1c shows that

further hydrothermal treatment for 24 hours of ZIF-8@polymer core-shell structured materials induced the generation of yolk-shell structured materials with inner diameters of about 365 nm and shell thickness of about 70 nm. Noticeably, it is also very interesting to find that nanoribbons are generated in the hollow polymer shell. A similar coating strategy was also introduced by Telfer et al. Resorcinol and formaldehyde were initially co-polymerized with the following addition of ZIF-8 nanoparticles to construct ZIF-8@polymer structure. HCl solution was used to etch ZIF-8 particles to obtain hollow polymer shell compared with our hydrothermal method of transforming ZIF-8 to ZnO.[28] The scanning transmission electron microscopy (STEM) and the corresponding energy dispersive X-ray spectroscopy (EDS) elemental mapping (Figure 1d) were obtained to identify the distribution of nitrogen, carbon, zinc and oxygen in this hollow structure. Elemental carbon and nitrogen are homogenously distributed in the carbon shell, but zinc and most oxygen atoms are present in the core materials only, indicating elemental zinc was confined in the hollow carbon shell. This confinement phenomenon can also be confirmed by coating polymer on the surface of ZIF-67 (Figure S2). To determine the yolk-shell structure of the ZnO@polymer, HAADF-STEM tomography was adapted. A 3D reconstruction of ZnO@polymer is shown in Figure 1e. In order to investigate the effect of polymer layer in the synthesis of ZIF-8@polymer, ZIF-8 particles were prepared without polymer coating. Figure S3 shows that the irregularly shaped particles with decreased average particle size of about 110 nm are only generated and nanoribbons are not observed, indicating that the polymer coating is essential for the formation of nanoribbons and the evolution of ZIF-8. For clarity, the TEM specimen of ZP particles is carefully tilted by rotation around the axis of the holder to -30° and +30°, as illustrated in Figure S4. The TEM images with multiple views reveal that the nanoribbon cores are indeed located in the inner shell.

After thermal treatment of ZP-100 in flowing nitrogen at 700 °C, the yolk-shell structured ZnO@carbon with shell thickness of about 45 nm were obtained (as shown in Figure 1f). As can be seen the calcination treatment disintegrates ZnO nanoribbons in the cores into small particles, which is probably derived from the chemical reduction reaction between ZnO core and the carbon capsule. Telfer and co-workers also found the evaporation of the zinc during the thermolysis of ZIF-8@polymer. [28] The scanning transmission electron microscopy (STEM) and the corresponding energy dispersive X-ray spectroscopy (EDS) elemental mapping (Figure 1g) are presented to identify the distribution of nitrogen, carbon, oxygen and zinc. As shown in Figure 1g, the elemental distribution is similar to that of ZP-100, indicating that the elemental zinc is confined inside of the hollow carbon. In order to know the formation of zinc evaporates, TGA-MS was used to monitor the gas products during the calcination of ZnO@polymer. MS measurement is only used to qualitatively trace the volatile species. As shown in Figure S5, it is clearly to see that zinc evaporates and CO_2 were detected from TG-MS profile, indicating that ZnO particles were partially reduced to zinc evaporates and CO_2. To quantify the elemental composition of zinc species in the ZnO@polymer and ZnO@carbon, ICP-OES was utilized. The results showed that the weight percentage of elemental zinc are 10.9% and 1.51%. Based on TG and ICP results, nearly 95% of ZnO particles were reduced.

We further demonstrate that Pd metal nanoparticles can be confined in the interior of yolk-shell structured ZnO@carbon to generate Pd&ZnO@carbon structures and also to investigate the chemical reaction between ZnO core particles and carbon capsule with Pd nanoparticels as catalysts as depicted in Scheme 1b. A similar polymer coating method, hydrothermal treatment followed by carbonization were used for the synthesis of Pd&ZnO@carbon. The Pd nanoparticles were obtained through wet-chemical reduction process in the presence of $NaBH_4$. The TEM images in Figure 2a and

HAADF images in Figure 2b and 2c show that highly-dispersed Pd metal nanoparticles have been successfully loaded on the surface of ZIF-8 particles. After coating polymer on the surface of metal-ZIF-8 and subsequent hydrothermal treatment, noble metal nanoparticles have been successfully incorporated in the shell of yolk-shell structured ZnO@polymer, as shown in Figure 2d. The polymer layer thickness of Pd&ZIF-8@polymer is 48 nm. To determine the dispersion of elements in Pd&ZnO@polymer, HAADF-STEM imaging and elemental mapping (Figure 2e) have been used to reveal that nitrogen atoms are homogeneously distributed in the polymer framework and metal nanoparticles have been successfully confined inside of polymer shell and on the surface of ZnO nanoribbons.

The as-prepared Pd&ZIF-8@polymer particles were carbonized in N_2 atmosphere to achieve Pd&ZnO@carbon. Thermal treatment of Pd&ZIF-8@polymer at 700 °C under inert environment resulted in volatilization and carbonization of the organic constituents and evaporation of zinc. As shown in TEM images (Figure 2f), small cubic clusters are present and nanoribbon structures are absent inside the hollow carbon structures with shell thickness of about 40 nm. This indicates that Pd nanoparticles play an important role as catalysts in chemical reactions between ZnO and carbon capsule. To determine the dispersion of elements in Pd&ZnO@carbon, HAADF-STEM imaging and elemental mapping (Figure 2g) were used to reveal that nitrogen atoms are homogeneously distributed in the carbon framework, zinc and oxygen atoms are visible in ZnO nanoparticles, and metal nanoparticles are also situated inside of carbon shells and on the surface of ZnO nanoparticles.

As a submicroreactor, ZIF-8 polyhedrons coated with resin polymer can be chemically converted to ZnO nanoribbon with higher reaction temperature. To further track the evolution of ZIF-8 polyhedrons@resin polymer during carbonization process, Pd metal nanoparticles were loaded onto

ZIF-8 before APF coating, and the conversion of ZIF-8 polyhedrons to ZnO was accelerated in presence of Pd as demonstrated in Figures 2f and g. The XRD measurements were performed to investigate the phase structure of ZnO@carbon (Figure 3a). Wurtzite ZnO (JCPDS 36-1451) is the only phase present in ZnO@carbon. The peaks around 25° probably can be attributed to amorphous carbon. The Brunauer–Emmett–Teller (BET) surface area and the pore volume obtained on the basis of the nitrogen adsorption isotherm (Figure 3b) are 621 $m^2 g^{-1}$ and 1.0 $cm^3 g^{-1}$, respectively. The XRD patterns in Figure 3c exhibit distinct reflections at 2θ of 41.5°, 44.3° and 64.6° for Pd&ZnO@carbon, which can be attributed to the (111), (200) and (220) peaks of face-centred cubic (FCC) Pd nanoparticles. The N_2 adsorption isotherm measured on Pd&ZnO@carbon shows type IV with steep H3 hysteresis loop (Figure 3d). The BET surface area and the pore volume are 445 $m^2 g^{-1}$ and 0.58 $cm^3 g^{-1}$, respectively. This indicates that the as-prepared Pd&ZnO@carbon particles possess abundant porous channels ensuring high permeation and mass transfer rates for species involved in a catalytic reaction.

In order to demonstrate the universality of this method, Au&ZnO@carbon and Pt&ZnO@carbon were synthesized by replacing Na_2PdCl_4 with $HAuCl_4 \cdot H_2O$ and H_2PtCl_6, respectively. Interestingly, both Au and Pt nanoparticles served as catalysts to accelerate the ZIF-8 conversion rate (Figure 4). Interestingly, Pt nanoparticles were dispersed well during the formation of carbon framework. A similar finding was also shown by Telfer et al.[28] The XRD patterns of Au&ZnO@carbon (Figure S6a) and Pt&ZnO@carbon (Figure S6c) exhibited characteristic peaks of Au and ZnO, Pt and ZnO, respectively. The N_2 adsorption isotherm measured on the Au&ZnO@carbon (Figure S6b) and Pt&ZnO@carbon (Figure S6d) shows type IV with steep H3 hysteresis loop, indicating the existence of micro-mesoporous structure. The BET surface area and the pore volume are 319 $m^2 g^{-1}$ and 0.34

$cm^3\ g^{-1}$, 477 $m^2\ g^{-1}$ and 0.6 $cm^3\ g^{-1}$, respectively. The Au and Pt weight loading of Au&ZnO@carbon and Pt&ZnO@carbon was about 2% through ICP analysis. The TEM images, HAADF images and element mapping images of their precursors including Au&ZnO@polymer and Pt&ZnO@polymer have also been shown in Figure S7 to further observe the transformation of ZnO particles. It is shown that the structural evolution of ZIF-8 polyhedrons in a confined space can be controlled by increasing reaction temperature or loading catalysts.

2.2. Catalytic performances

In order to evaluate the catalytic performance of the as-prepared Pd&ZnO@carbon particles, the selective hydrogenation of phenylacetylene to phenylethylene was performed at 30 °C under 1 bar of H_2 over a period of 80 minutes. As shown in Figure 5a, the catalytic activity of Pd-encapsulated ZnO@carbon particles was superior (conversion 96% and selectivity 99%). As compared with the Pd&ZnO@carbon particles, Pd/ZnO particles (Figure S8) (conversion 43%) and Pd/carbon particles (Figure S9) (conversion 56%) show relatively lower hydrogenation efficiency (with the same Pd loading) and selectivity in the hydrogenation of phenylacetylene. The Pd weight loading of the comparable samples including Pd&ZnO@carbon, Pd/C and Pd/ZnO was about 2% through ICP analysis. As shown in Figure S10, the conversion of Au&ZnO@carbon and Pt&ZnO@carbon nanoparticles for catalytic hydrogenation behaviour proved to be 20% and 86% with similar selectivity (99%). In general, several factors including particle composition, size and the nature of the support materials are of great importance for catalysts performance.[46-49] As to this novel

Pd&ZnO@carbon composite, the high phenylacetylene conversion is probably ascribed to the carbon submicroreactor, which can enrich the phenylacetylene accumulation by confinement effect, enhancing the collision frequency and adsorption of phenylacetylene on the Pd nanoparticles surface.[50] Meanwhile, ZnO nanoparticles in-situ embedded inside the carbon submicroreactor provide a basic environment which can promote desorption of phenylethylene and prohibit its over-hydrogenation.[51] Therefore, the high phenylacetylene conversion and phenylethylene selectivity over Pd&ZnO@carbon catalyst can be attributed to the unique multi-functional reactor benefiting both the adsorption of phenylacetylene and the desorption of phenylethylene during the selective hydrogenation reaction.

The recycling stability of a catalyst is important in practical applications. To evaluate the reusability of Pd&ZnO@carbon, five consecutive cycles were carried out and the reaction time in each cycle was fixed at 80 min. As shown in Figure 5b, both conversion activity and selectivity of Pd&ZnO@carbon in 5 cycles are maintained, with a selectivity of about 99% for phenylacetylene and conversion of around 95.5%. However, as shown in Figure 5b, the initial conversion of Pd/ZnO and Pd/carbon catalysts are 43.2% and 56.2% and they decrease gradually with each reaction. Only 5.5 %and 9.5% conversion of Pd/ZnO and Pd/carbon catalysts are obtained after 5 runs. The superior catalytic stability of Pd&ZnO@carbon can also be demonstrated through CO oxidation, as shown in Figure S11, indicating no deactivation occurs for Pd&ZnO@carbon catalysts when the catalytic reaction is performed at 120°C for 25h with CO conversion ratio about 90%. These results indicate the good stability of the Pd&ZnO@carbon catalyst, which make them promising catalysts for the selective hydrogenation of phenylacetylene. This reveals that there are no obvious variations in the size,

shape and yolk-shell nanostructures, and the carbon shells effectively encapsulate the active noble metal cores and prevent leaching or severe particle agglomeration.

2.3 Morphology evolution via hydrothermal treatment

To understand the formation mechanism of yolk-shell structured ZnO@polymer, the effect of polymer amount, initial synthesis temperatures and reaction time on the morphology evolution of ZnO nanoparticles was investigated. The sequence of TEM images, HRTEM images, SAED patterns and XRD patterns (Figure 6, S12-S15) corresponding to the formation of nanoribbons and their growth at different hydrothermal reaction time and temperature provide some insight into the formation of yolk-shell structure. ZIF-8 particles with sodalite topology were consisted with tetrahedral Zn ions bridged by imidazolate linkages.[22] As shown in Figure S12, hydrothermal treatment for 3h and 12 h results in the shrinkage and dissolution of the ZIF-8 core and the partial transformation from polyhedron structure to small nanoparticles, revealing that the prolonged thermal treatment breaks Zn-N coordination bonds, which starts dissolution of Zn-imidazole framework and further formation of amorphous nanoparticles. It is very clear that the voids between the cores and shells start to form asymmetrically, also indicating the region of the edge of ZIF-8 is less dense or easier to decompose than the centre. This is obvious from the produced dark and amorphous nanoparticles visible on the TEM image (in Figure S12). Until hydrothermal treatment for 24 h, the well-defined nanoribbons are generated.

TEM images in Figures S13 and S14 depict the impact of hydrothermal temperature on the morphology of ZnO nanoribbons. Hydrothermal treatment at lower temperature such as 60 °C induces the conversion from polyhedron-structured ZIF-8 particles into needle-like structure. When

increasing the hydrothermal temperature to above 100 °C, the polymer shell thickness decreases, which results in faster heat transfer from the outside solution to the inner core and the total dissolution of ZIF-8 at 140 °C. The conversion from Zn-N coordination bonds to Zn-O covalent bonds is completed at relatively high temperatures such as 140 °C. The composite XRD pattern at different hydrothermal temperatures highlights the formation of nanoribbon of these samples. From Figure 6a, the XRD profiles of the samples obtained at 100 °C and 120 °C display additional peaks as compared to those recorded for the sample prepared at 60 °C, which reflect the formation of wurtzite ZnO (JCPDS 36-1451). After hydrothermal treatment at 140 °C, the peaks of ZIF-8 totally disappear, indicating that the complete transformation from ZIF-8 to ZnO nanoribbons. HRTEM and SAED (Figure 6b, Figure S13b and Figure S13c) of ZP-60, ZP-100 and ZP-140 for different temperatures provide further details on the crystal growth during synthesis. HRTEM analysis of nanoribbon structures present in the sample prepared at 100 °C (Figure 6b) indicates that the calculated lattice spacing are 0.52 nm, 0.26 nm and 0.25 nm, which can be ascribed to (001), (002) and (101) crystal planes of ZnO, respectively. The SAED patterns (inset in Figure 6b) also reveal the presence of these crystal planes, which is also confirmed by XRD patterns in Figure 6a. Formation of zinc oxide can be described by the following chemical reactions during hydrothermal treatment:

ZIF-8 ($Zn(MI)_2$) + $2H_2O$ = $Zn(OH)_2$ + 2HMI (1)

$Zn(OH)_2$ = ZnO + H_2O (2)

Where MI and HMI denote imidazolate ligand and 2-methylimidazole.

Therefore, ZnO nanoribbon evolution occurs via the dissolution of ZIF-8 and formation of the intermediate needle-like particles.

3. Conclusions

In summary, we demonstrated the facile synthesis of yolk-shell particles with controllable chemical compositions, spatial locations of active components, and tuneable shell layers. Multicomponent yolk-shell structured ZnO@polymer particles were prepared through coating polymer and subsequent hydrothermal treatment. Yolk-shell structured ZnO@carbon can be generated through the carbonization process of ZnO@polymer particles. ZnO nanoribbon evolution is observed to occur via disintegration of ZIF-8 and formation of the intermediate needle-like particles. The as-prepared Pd&ZnO@carbon particles are catalytically active and stable in the hydrogenation of phenylacetylene reaction. The outstanding catalytic performance of Pd-encapsulated ZnO@carbon particles is evidenced by much higher conversion and selectivity than that obtained for Pd/ZnO and Pd/C with the similar Pd loading and superior selectivity, stability and reusability. The nanoconfinement effect discussed in this work may open up new prospects for the applications of multiple functionalized YSNs as efficient nanoreactors for various applications.

4. Experimental Section

Synthesis of ZnO@polymer (ZP)

In a typical synthesis, CTAB (0.1 g) was dissolved in a mixture of water (20 mL) and ethanol (8 mL). Then, an aqueous solution of ammonia (NH_4OH, 0.2 mL, 25 wt%) was added and stirred at room temperature for 0.5 h, followed by addition of 0.1g of ZIF-8. After stirring for 0.5h, 3-aminophenol (0.08 g) was added into that suspension and stirring was continued for an additional 30 min. Next, a solution of formaldehyde (0.11 mL) was added. The mixture was stirred for 24 h at room

temperature and subsequently heated for 24 h at 100 °C under static conditions in a Teflon-lined autoclave. The solid product was recovered by centrifugation and dried at 100 °C for 24 h. Subsequent variations of the synthesis process involved alteration of the hydrothermal treatment time for 3 and 12 h, respectively (giving the following samples: ZP-3h and ZP-12h), hydrothermal temperature at 60 °C, 80 °C, 120 °C, 140 °C (giving the samples: ZP-60, ZP-80, ZP-120 and ZP-140), and the amount of 3-aminophoneol, 0.04 and 0.12 g, respectively (giving the samples: ZP-1 and ZP-2).

Supporting Information

Supporting Information is available from the Wiley Online Library or from the author.

Acknowledgements

The authors acknowledge the Curtin University Electron Microscope Laboratories, partially funded by the University, State and Commonwealth Governments. The authors also wish to thank the Australian Microscopy & Microanalysis Research Facility at the Centre for Microscopy, Characterisation & Analysis, the University of Western Australia, funded by the University, State and Commonwealth Governments. This work was financially supported by the Australian Research Council (ARC) through Discovery Project program (DP180100568) and Linkage Project program (LP150101158). J.L. gratefully acknowledges the support of Chinese Government 1000 young talent plan. H.T. gratefully acknowledges the support of Curtin Strategic International Research Scholarship, Curtin University Mobility Scholarship and Chinese Government Award for Outstanding Self-Financed Students Abroad. H.T. would also like to thank Prof. Martin Saunders and Dr Aaron Dodd

for TEM training from CMCA in UWA and Dr Chi Zhang for XRD test. H.L. acknowledges the Ministry of Science and Technology (2016YFA0204100), the National Natural Science Foundation of China (21573254 and 91545110), the Youth Innovation Promotion Association(CAS), and the Sinopec China. The authors would like to thank Prof. Can Li for fruitful discussions.

Received: ((will be filled in by the editorial staff))
Revised: ((will be filled in by the editorial staff))
Published online: ((will be filled in by the editorial staff))

[1] Y.-X. Wang, J. Yang, S.-L. Chou, H. K. Liu, W.-x. Zhang, D. Zhao, S. X. Dou, *Nature Commun.* **2015**, *6*, 8689.

[2] Z. Li, J. Zhang, B. Guan, D. Wang, L.-M. Liu, X. W. Lou, *Nature Commun.* **2016**, *7*, 13065.

[3] J. Liu, H. Q. Yang, F. Kleitz, Z. G. Chen, T. Yang, E. Strounina, G. Q. Lu, S. Z. Qiao, *Adv. Funct. Mater.* **2012**, *22*, 591-599.

[4] Z. Teng, X. Su, Y. Zheng, J. Zhang, Y. Liu, S. Wang, J. Wu, G. Chen, J. Wang, D. Zhao, G. Lu, *J. Am. Chem. Soc.* **2015**, *137*, 7935-7944.

[5] J. Liu, S. Z. Qiao, J. S. Chen, X. W. Lou, X. Xing, G. Q. Lu, *Chem. Comm.* **2011**, *47*, 12578-12591.

[6] H. Tian, M. Saunders, A. Dodd, K. O'Donnell, M. Jaroniec, S. Liu, J. Liu, *J. Mater. Chem. A* **2016**, *4*, 3721-3727.

[7] J. Liu, S. Z. Qiao, S. Budi Hartono, G. Q. Lu, *Angew. Chem. Int. Ed.* **2010**, *122*, 5101-5105.

[8] Y. Chen, H. Chen, L. Guo, Q. He, F. Chen, J. Zhou, J. Feng, J. Shi, *ACS Nano* **2010**, *4*, 529-539.

[9] S. Ding, J. S. Chen, G. Qi, X. Duan, Z. Wang, E. P. Giannelis, L. A. Archer, X. W. Lou, *J. Am. Chem. Soc.* **2011**, *133*, 21-23.

[10] B. Liu, H. C. Zeng, *Small* **2005**, *1*, 566-571.

[11] E. C. Cho, P. H. C. Camargo, Y. Xia, *Adv. Mater.* **2010**, *22*, 744-748.

[12] Y. D. Yin, R. M. Rioux, C. K. Erdonmez, S. Hughes, G. A. Somorjai, A. P. Alivisatos, *Science* **2004**, *304*, 711-714.

[13] R. Banerjee, A. Phan, B. Wang, C. Knobler, H. Furukawa, M. O'Keeffe, O. M. Yaghi, *Science* **2008**, *319*, 939-943.

[14] K. S. Park, Z. Ni, A. P. Cote, J. Y. Choi, R. D. Huang, F. J. Uribe-Romo, H. K. Chae, M. O'Keeffe, O. M. Yaghi, *Proc. Natl. Acad. Sci. USA* **2006**, *103*, 10186-10191.

[15] R. R. Salunkhe, Y. V. Kaneti, J. Kim, J. H. Kim, Y. Yamauchi, *Acc. Chem. Res.* **2016**, *49*, 2796-2806.

[16] Y. V. Kaneti, J. Tang, R. R. Salunkhe, X. Jiang, A. Yu, K. C. W. Wu, Y. Yamauchi, *Adv. Mater.* **2017**, *29*, 1604898.

[17] S. Dang, Q.-L. Zhu, Q. Xu, *Nature Rev. Mater.* **2017**, *3*, 17075.

[18] C. H. Kuo, Y. Tang, L. Y. Chou, B. T. Sneed, C. N. Brodsky, Z. P. Zhao, C. K. Tsung, *J. Am. Chem. Soc.* **2012**, *134*, 14345-14348.

[19] F. Zhang, Y. Y. Wei, X. T. Wu, H. Y. Jiang, W. Wang, H. X. Li, *J. Am. Chem. Soc.* **2014**, *136*, 13963-13966.

[20] H. Hu, B. Guan, B. Xia, X. W. Lou, *J. Am. Chem. Soc.* **2015**, *137*, 5590-5595.

[21] J. Zhang, H. Hu, Z. Li, X. W. Lou, *Angew. Chem. Int. Ed.* **2016**, *55*, 3982-3986.

[22] J. Yang, F. J. Zhang, H. Y. Lu, X. Hong, H. L. Jiang, Y. Wu, Y. D. Li, *Angew. Chem. Int. Ed.* **2015**, *54*, 10889-10893.

[23] J. Tang, R. R. Salunkhe, J. Liu, N. L. Torad, M. Imura, S. Furukawa, Y. Yamauchi, *J. Am. Chem. Soc.* **2015**, *137*, 1572-1580.

[24] G. Lu, S. Li, Z. Guo, O. K. Farha, B. G. Hauser, X. Qi, Y. Wang, X. Wang, S. Han, X. Liu, J. S. DuChene, H. Zhang, Q. Zhang, X. Chen, J. Ma, S. C. J. Loo, W. D. Wei, Y. Yang, J. T. Hupp, F. Huo, *Nat. Chem.* **2012**, *4*, 310-316.

[25] M. Zhao, K. Yuan, Y. Wang, G. Li, J. Guo, L. Gu, W. Hu, H. Zhao, Z. Tang, *Nature* **2016**, *539*, 76-80.

[26] P. Yin, T. Yao, Y. Wu, L. Zheng, Y. Lin, W. Liu, H. Ju, J. Zhu, X. Hong, Z. Deng, G. Zhou, S. Wei, Y. Li, *Angew. Chem. Int. Ed.* **2016**, *55*, 10800-10805.

[27] J. Yang, F. Zhang, X. Wang, D. He, G. Wu, Q. Yang, X. Hong, Y. Wu, Y. Li, *Angew. Chem. Int. Ed.* **2016**, *55*, 12854-12858.

[28] H. Yang, S. J. Bradley, A. Chan, G. I. N. Waterhouse, T. Nann, P. E. Kruger, S. G. Telfer, *J. Am. Chem. Soc.* **2016**, *138*, 11872-11881.

[29] H. Yang, S. J. Bradley, X. Wu, A. Chan, G. I. N. Waterhouse, T. Nann, J. Zhang, P. E. Kruger, S. Q. Ma, S. G. Telfer, *ACS Nano* **2018**, 10.1021/acsnano.8b01022

[30] H. Liu, C. Y. Xu, D. D. Li, H. L. Jiang, *Angew. Chem. Int. Ed.* **2018**, *57*, 5379-5383.

[31] H. J. Xu, J. Cao, C. F. Shan, B. K. Wang, P. X. Xi, W. S. Liu, Y. Tang, *Angew. Chem. Int. Ed.* **2018**, 10.1002/anie.201804673.

[32] L. Yang, X. F. Zeng, W. C. Wang, D. P. Cao, *Adv. Funct. Mater.* **2018**, *28*, 1704537

[33] M. D. Zhang, Q. B. Dai, H. G. Zheng, M. D. Chen, L. M. Dai, *Adv. Mater.* **2018**, *30*, 1705431

[34] Y. Pan, R. Lin, Y. J. Chen, S. J. Liu, W. Zhu, X. Cao, W. X. Chen, K. L. Wu, W. C. Cheong, Y. Wang, L. Zheng, J. Lu, Y. Lin, Y. Q. Liu, C. G. Liu, J. Li, Q. Lu, X. Chen, D. S. Wang, Q. Peng, C. Chen, Y. D. Li, *J. Am. Chem. Soc.*, **2018**, *140*, 4218-4221

[35] L. Jiao, Y. Wang, H.-L. Jiang, Q. Xu, *Adv. Mater.* **2017**, 1703663.

[36] B. Y. Xia, Y. Yan, N. Li, H. B. Wu, X. W. Lou, X. Wang, *Nature Energy* **2016**, *1*, 15006.

[37] J. Liu, S. Z. Qiao, H. Liu, J. Chen, A. Orpe, D. Zhao, G. Q. Lu, *Angew. Chem. Int. Ed.* **2011**, *50*, 5947-5951.

[38] J. Liu, T. Yang, D.-W. Wang, G. Q. Lu, D. Zhao, S. Z. Qiao, *Nature Commun.* **2013**, *4*, 2798.

[39] J. Liu, N. P. Wickramaratne, S. Z. Qiao, M. Jaroniec, *Nat. Mater.* **2015**, *14*, 763-774.

[40] T. Yang, R. Zhou, D.-W. Wang, S. P. Jiang, Y. Yamauchi, S. Z. Qiao, M. J. Monteiro, J. Liu, *Chem. Comm.* **2015**, *51*, 2518-2521.

[41] T. Yang, J. Liu, Y. Zheng, M. J. Monteiro, S. Z. Qiao, *Chem.-Eur. J.* **2013**, *19*, 6942-6945.

[42] J. Zhang, K. Wang, Q. Xu, Y. Zhou, F. Cheng, S. Guo, *ACS Nano* **2015**, *9*, 3369-3376.

[43] H. Tian, H. Liu, T. Yang, J.-P. Veder, G. Wang, M. Hu, S. Wang, M. Jaroniec, J. Liu, *Materials Chemistry Frontiers* **2017**, *1*, 823-830.

[44] T. Yang, H. Ling, J.-F. Lamonier, M. Jaroniec, J. Huang, M. J. Monteiro, J. Liu, *NPG Asia Mater.* **2016**, *8*, e240

[45] W. Zhang, Y. Liu, G. Lu, Y. Wang, S. Li, C. Cui, J. Wu, Z. Xu, D. Tian, W. Huang, J. S. DuCheneu, W. D. Wei, H. Chen, Y. Yang, F. Huo, *Adv. Mater.* **2015**, *27*, 2923-2929.

[46] G.-H. Wang, J. Hilgert, F. H. Richter, F. Wang, H.-J. Bongard, B. Spliethoff, C. Weidenthaler, F. Schüth, *Nature Mater.* **2014**, *13*, 293.

[47] H. Liu, L. Zhang, N. Wang, D. S. Su, *Angew. Chem. Int. Ed.* **2014**, *53*, 12634-12638.

[48] H.-U. Blaser, H. Steiner, M. Studer, *ChemCatChem* **2009**, *1*, 210-221.

[49] Z. Li, M. Li, Z. Bian, Y. Kathiraser, S. Kawi, *Appl. Catal., B* **2016**, *188*, 324-341.

[50] J.-M. Nhut, L. Pesant, J.-P. Tessonnier, G. Winé, J. Guille, C. Pham-Huu, M.-J. Ledoux, *Appl. Catal., A.* **2003**, *254*, 345-363.

[51] Y. Zhang, J. Wang, J. Rong, J. Diao, J. Zhang, C. Shi, H. Liu, D. Su, *ChemSusChem* **2017**, *10*, 353-358.

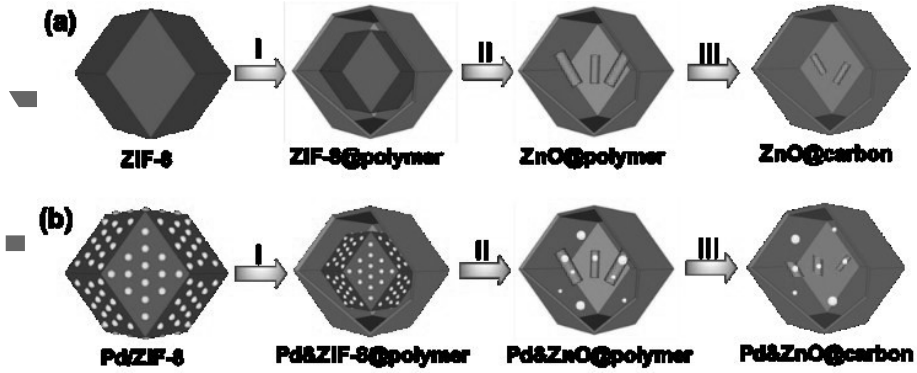

Scheme 1 Schematic illustration of the fabrication of yolk-shell structured ZnO@carbon (ZC) (a) and Pd&ZnO@carbon (b): I) uniform coating of polymer onto the surface of ZIF-8 and Pd/ZIF-8; II) hydrothermal treatment of ZIF-8@polymer and Pd&ZIF-8@polymer; III) carbonization in nitrogen atmosphere. (Blue, purple, yellow, green and grey colours refer to ZIF-8, polymer layer, metal nanoparticles, ZnO particles and carbon layer, respectively

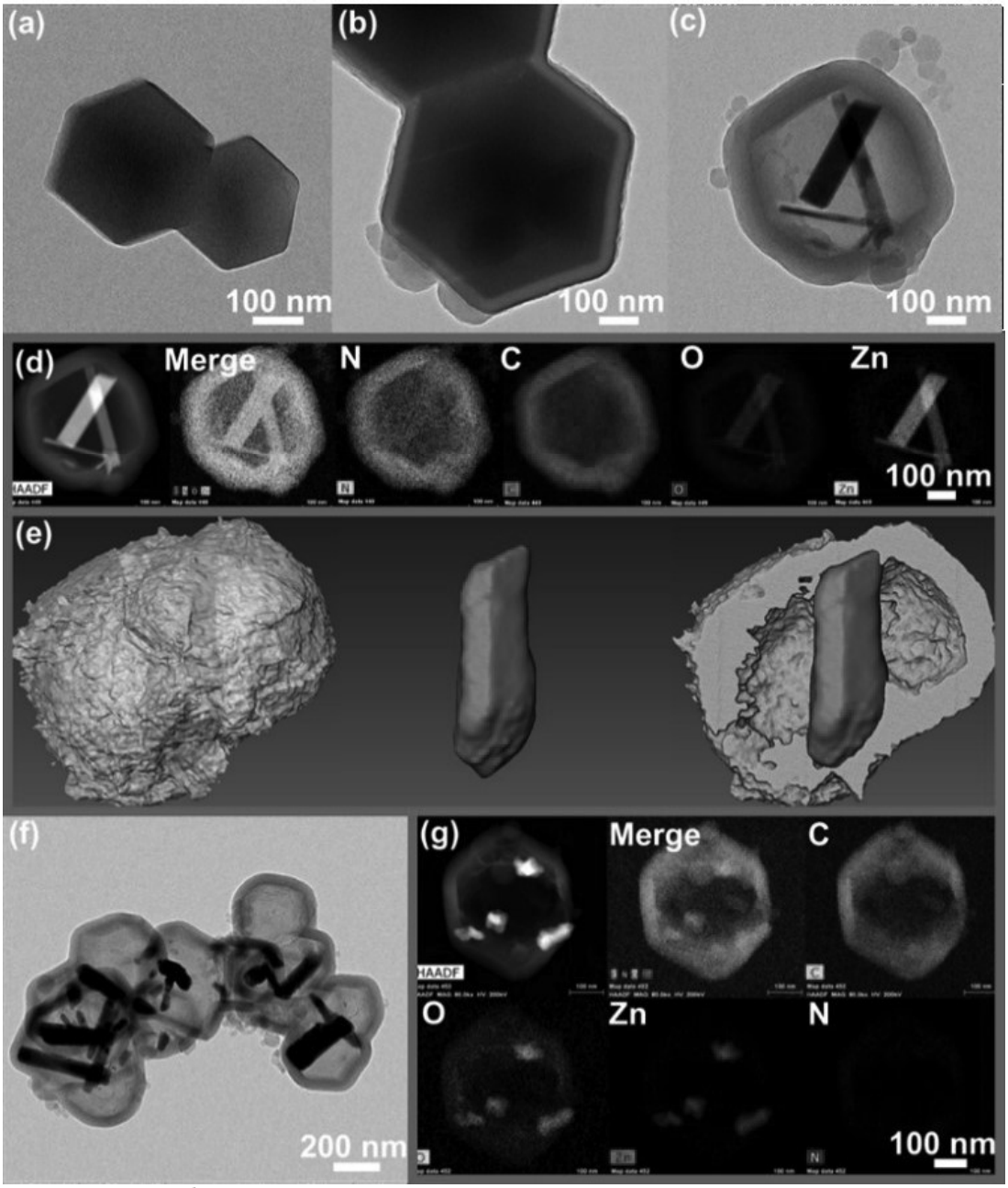

Figure 1 TEM images of (a) ZIF-8, (b) ZIF-8@polymer before hydrothermal treatment, (c) TEM image, (d) STEM image and EDS mapping of ZP-100, (e) 3D representation of the ZP-100 reconstruction. (f)TEM image, STEM and EDS mapping (g) of ZnO@carbon.

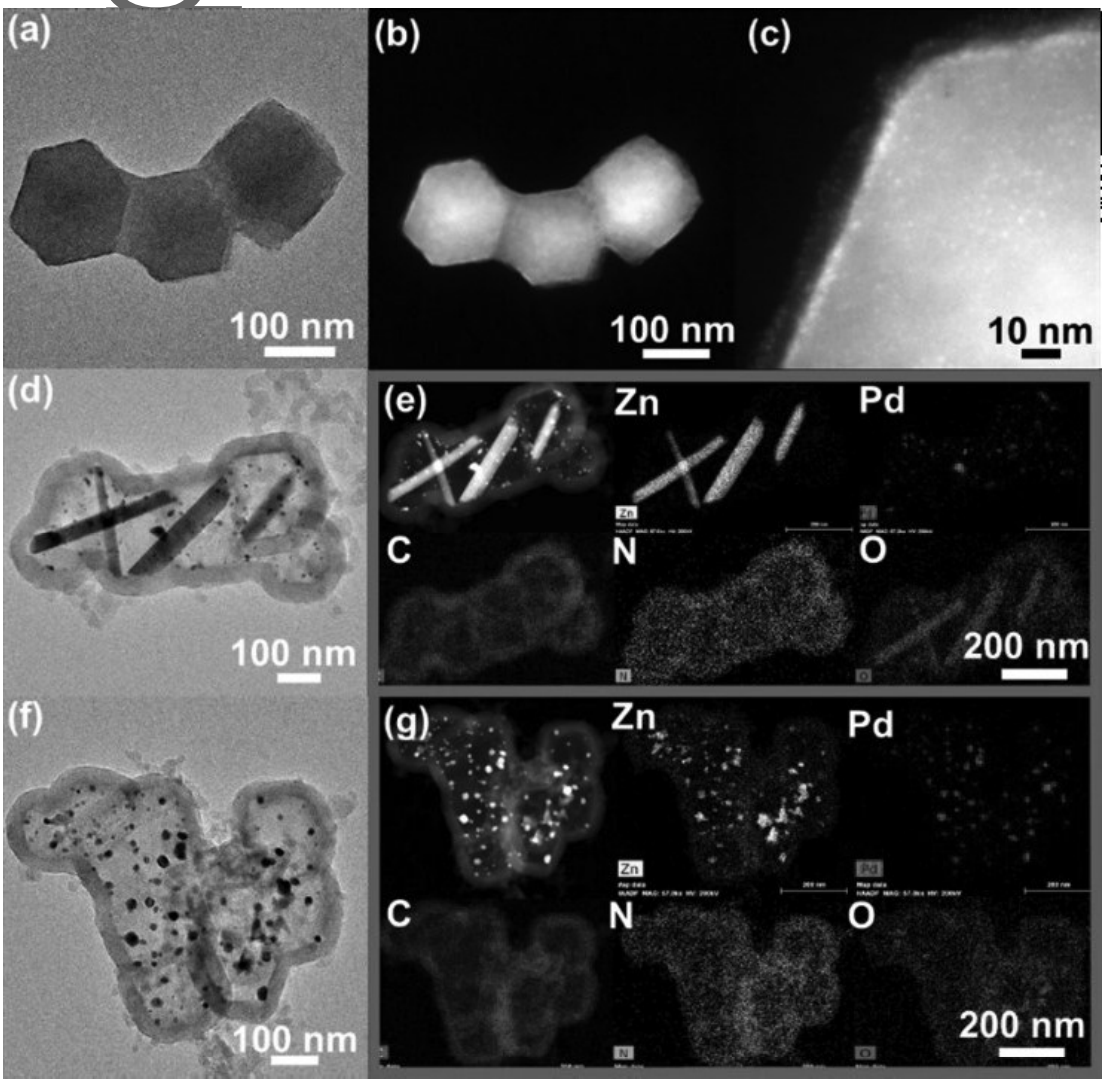

Figure 2 TEM image (a), HAADF images (b) (c) of Pd/ZIF-8; TEM image (d) and elemental mapping images (e) of Pd&ZnO@polymer; TEM image (f) and elemental mapping images (g) of Pd&ZnO@carbon.

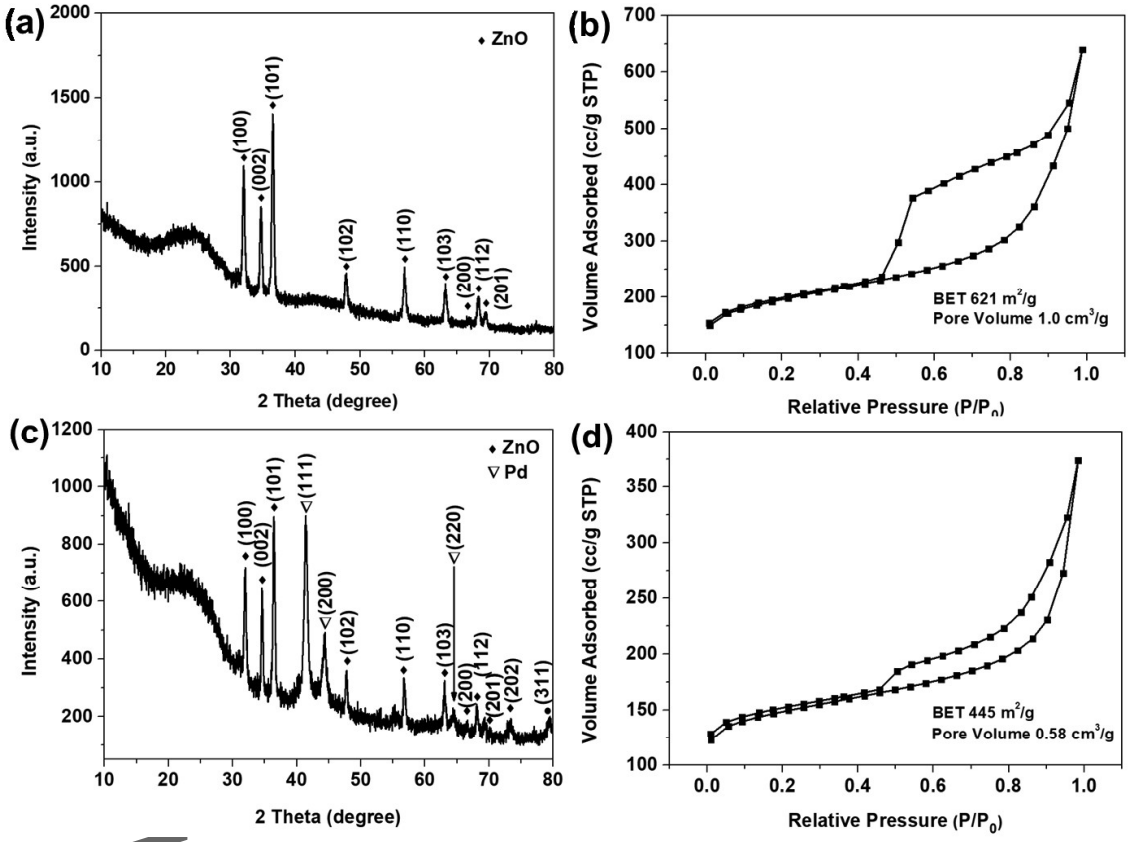

Figure 3 XRD patterns (a) (c) and N_2 adsorption–desorption isotherm (b) (d) of ZnO@carbon and Pd&ZnO@carbon.

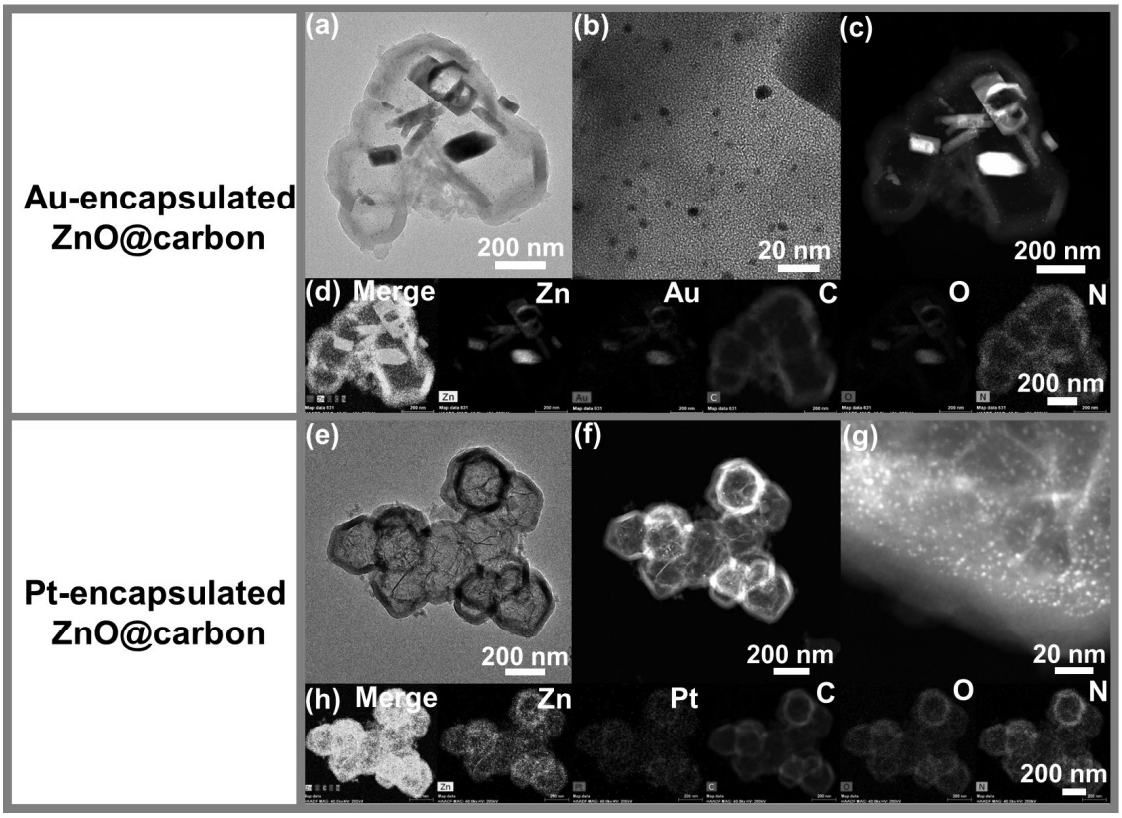

Figure 4 TEM images (a) (b), HAADF images(c), elemental mapping images (d) of Au&ZnO@carbon; TEM images (e), HAADF images (f) (g), elemental mapping images (h) of Pt&ZnO@carbon.

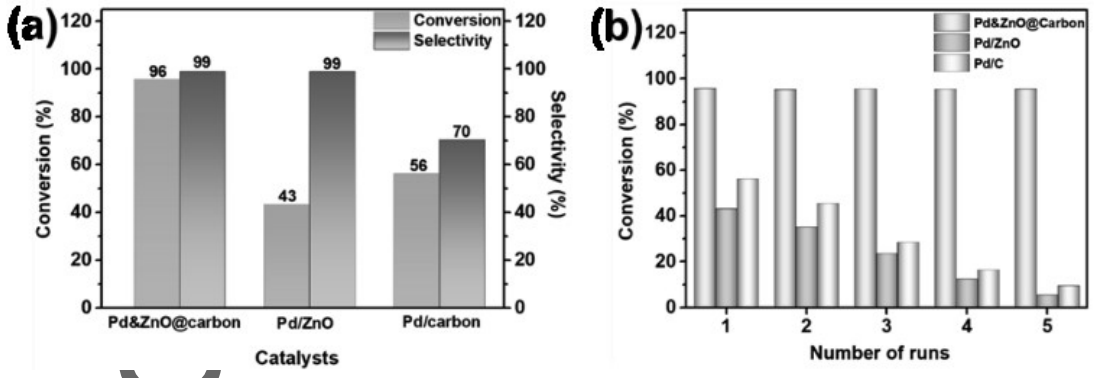

Figure 5 (a) Conversion and selectivity to phenylacetylene hydrogenation;(b) recycling tests for Pd&ZnO@carbon, Pd/ZnO and Pd/C particles. (Standard conditions: 30 °C; 60 min; 20 mg of catalyst; 1 bar H_2; 2.9 mmol of substrate; 25 mL of ethanol as solvent.)

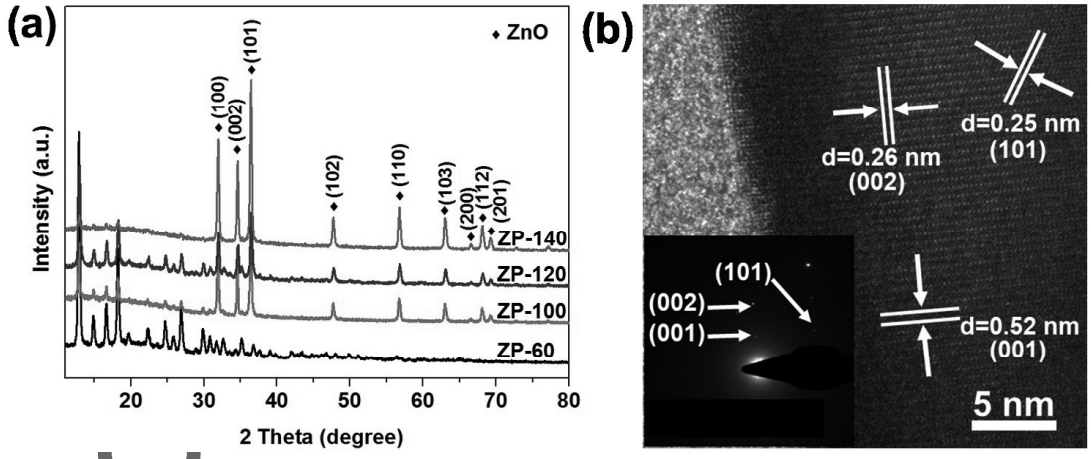

Figure 6 (a) XRD patterns of ZP-60, ZP-100, ZP-120, ZP-140; (b) HRTEM image of ZP-100 with its corresponding SAED pattern).

The table of contents

A unique transformation of Pd/ZIF-8@polymer is achieved under hydrothermal conditions to generate unique Pd&ZnO@polymer submicroreactors, which were used to generate Pd&ZnO@carbon yolk-shell submicroreactors. They exhibit enhanced high catalytic activity and selectivity in the semi-hydrogenation of phenylacetylene.

Keyword

submicroreactor, yolk-shell, metal–organic frameworks, phenylacetylene hydrogenation, zeolite imidazolate frameworks.

Title (The development of yolk-shell structured Pd&ZnO@carbon submicroreactors with high selectivity and stability)

TOC Figure